

STATISTICAL FAULT DETECTION AND IDENTIFICATION IN AIRCRAFT SYSTEMS VIA FUNCTIONALLY POOLED NONLINEAR MODELLING OF FLIGHT DATA DEPENDENCIES

Dimitrios G. Dimogianopoulos, John D. Hios, and Spilios D. Fassois

Stochastic Mechanical Systems & Automation (SMSA) Group, Department of Mechanical & Aeronautical Engineering, University of Patras, GR 265 00 Patras, Greece, Tel/Fax: (++ 30) 2610 997 405, E-mail: {dimogian, hiosj, fassois}@mech.upatras.gr, <http://www.mech.upatras.gr/~sms>

Keywords: *Fault detection and identification, aircraft systems, statistical methods*

Abstract

A Fault Detection and Identification (FDI) scheme for aircraft systems based on the modelling of relationships among flight variables is introduced. The modelling is performed by means of Time-dependent Functionally Pooled Nonlinear AutoRegressive with eXogenous (TFP-NARX) excitation representations. These are generalized NARX representations with (a) their parameters being functions of time-dependent flight variables and (b) the capability of describing a system under various operating conditions due to their pooled form. During the system's operation in healthy mode, these relationships are valid. Hence a scheme using statistical hypothesis testing is designed to detect changes in the relationships due to potential fault occurrence. The FDI scheme's performance and robustness are assessed with flights conducted under various flight conditions.

1 Introduction

The critical requirements of reliability and security in modern aircraft systems should be obtained at the lowest possible cost. The replication of existing critical hardware (the “hardware redundancy” principle) coupled to a voting scheme to perform Fault Detection and Identification (FDI) implies added weight and cost, while its

reliability is often criticized [1]. Hence, a new family of FDI schemes based upon the intelligent use of the existing hardware has emerged.

Examples may be found in [2], [3], [4] and [5]. The schemes in [2], [3] and [4] are based upon the Interactive Multiple Model (IMM) principle: Kalman filters provide linear “healthy” and “faulty” models for the sensors and actuators considered, and the one corresponding to the current aircraft state is selected by means of a probabilistic principle. The work in [5] relies on the Multiple Model Switching and Tuning (MMST) concept to provide linear adaptive models, each one covering an area of the aircraft dynamics under specific failure scenarios. All model outputs are used to find the model closest to the current plant dynamics, switch to that one and adapt from there. Although complicated (many filters per component, adaptive design), the application of these schemes is reportedly successful.

In [1] (and the references therein), FDI filters are designed using the \mathcal{H}_∞ principle for open loop, linear time invariant models of the aircraft (Boeing 747 100/200, on which validation is also carried out) to detect and isolate faults in the elevator actuator and pitch rate sensors. The \mathcal{H}_∞ approach minimizes the influence of noise, disturbances and so on, while maximizing the effects of faults. However, it relies on knowledge of the appropriate transfer functions of the aircraft under

consideration. To avoid using detailed aircraft models for FDI, a *weak model-based* approach is introduced in [6]. A single sensor signal (Angle-of-Attack) is processed by non-stationarity removal and by whitening via a suitably estimated filter (*weak model* approach). Then, using statistical decision making on the resulting signal allows for the detection of abrupt sensor faults. The method is successfully validated with real data.

Other FDI designs taking into account the highly nonlinear nature of the aircraft dynamics are Neural Network (NN) based methods [7], [8], [9]. The detection of a failed sensor is based upon monitoring the difference between the (sensor-obtained) signal and its estimated counterpart (obtained from the identified NN models). The NN models capture the nonlinear aircraft dynamics with good precision, but with a high level of complexity and time consuming training. Alternative FDI approaches are based upon the existence of specific relationships among physical system variables. In [10], for instance, FDI on an Unmanned Aerial Vehicle (UAV) fuel (sub)system is based upon such relationships provided by physics based modelling. Since these relationships are valid as long as the system is in its healthy state, any changes are indicative of fault occurrence.

The aim of this study is the design and feasibility assessment of a statistical FDI scheme based upon the processing of available flight quantities (accelerations, pitch rate and so on). The scheme relies on the structural dependencies among these quantities, for which (unlike the applications in [10] or [11]) a physical model may not be available or may be very complex. These dependencies are valid as long as the aircraft operates in healthy state. They are modelled by means of Time-dependent Functionally Pooled Nonlinear AutoRegressive with eXogenous (TFP-NARX) excitation representations (see [12] on pooled models). These may be thought of as generalizations of conventional NARX representations, with two extra features: (a) Their parameters are functions of specific time-dependent flight variables. (b) They are capable of describing a system under various oper-

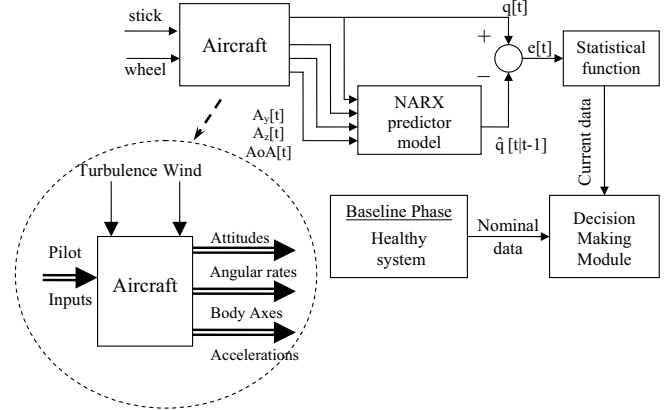


Fig. 1 : The fault detection and identification scheme and aircraft simulator detail.

ating conditions using multiple data records, due to their pooled form.

The use of *pooling techniques* (presented in section 3.1) means that all recorded data corresponding to different flight conditions (that is, flights conducted under various turbulence levels, altitude, Mach numbers and so on) are taken into account during the representation building phase. Furthermore, linking the parameters to specific flight variables leads to a more “flexible” (and accurate) representation of the modelled relationships throughout the considered flight regime. When the aircraft is affected by faults, the identified model provides useful fault-related information, which is subsequently evaluated by means of statistical hypothesis testing. The proposed scheme is tested with a large number of flights obtained by a nonlinear aircraft simulator, under various environmental conditions (turbulence).

2 The Aircraft and The Faults

The aircraft system considered is a 6 Degree-Of-Freedom (DOF) nonlinear aircraft simulator. Inputs are the pilot commands (stick, wheel and pedal), and outputs are the attitudes, the accelerations and the angular rates (see Fig. 1). The wind and turbulence effects are considered as system disturbances.

This study concentrates on faults of various magnitudes affecting the elevator and the aileron subsystems. The faults are injected into the sys-

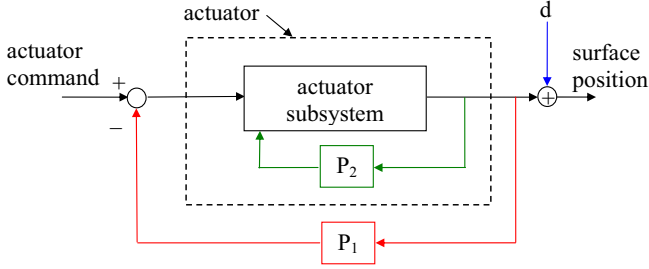


Fig. 2: Generic representation of the elevator/aileron primary and secondary circuits.

Table 1. The faults considered.

Type	Description	Magnitude
F_k^A	Elevator LOE	$k \in [0.03, 0.44]$
F_k^B	Noise in Aileron	$k = 0.1, 0.25, 0.5$
F_{k_1, k_2}^C	2× Elevator LOE	$k_1 = 0.001, k_2 = 0.03$
F_{k_1, k_2}^D	Elevator & Aileron LOE	$k_1 = 0.001$ $k_2 \in [0.03, 0.44]$

tem by modifying the corresponding component blocks in the aircraft simulator and are summarized in Table 1. In the following paragraphs, each fault type is presented in detail.

Elevator Faults: These LOE (Loss of Effectiveness) faults describe equipment deterioration (for instance, a non properly functioning actuator circuit). A generic representation of an actuator circuit (applicable to both the elevator and aileron circuits) is presented in Fig. 2. Each such fault is designated as F_k^A with A indicating the elevator subsystem and k the specific fault magnitude. The elevator faults are created in the aircraft simulator by reducing the position feedback gain P_1 (see Fig. 2) of the left elevator, from 1 in the healthy case to the values shown in Table 1. In Fig. 3(a) the aircraft pitch rate response is compared for a healthy and a faulty (affected by a $F_{0.3}^A$ fault) elevator, for a pilot stick input of 15 lbs step at $t = 5$ sec, with wheel and pedal inputs equal to zero in the landing flight regime. The overall reduction of the elevator effectiveness is small and the aircraft can still fly safely.

Aileron Faults: These correspond to a small vibration of the aileron surface that may result from a slightly deteriorating actuator. They are

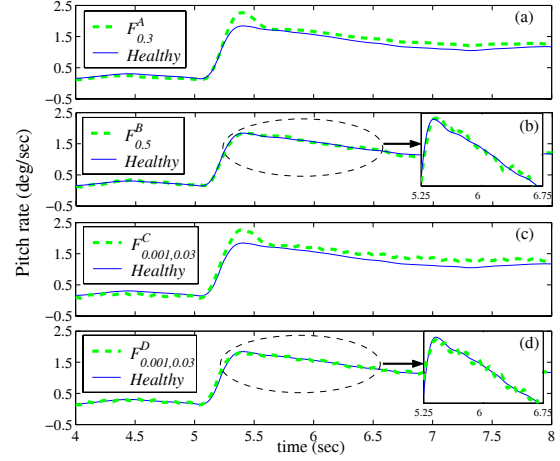


Fig. 3: Aircraft pitch rate responses for a stick input of 15 lbs at 5 sec: (a) Healthy versus $F_{0.3}^A$ affected ; (b) healthy versus $F_{0.5}^B$ affected; (c) healthy versus $F_{0.001, 0.03}^C$ affected and (d) healthy versus $F_{0.001, 0.03}^D$ affected (low turbulence, landing flight regime).

created by means of a small additive white noise applied on the left aileron deflection (shown as the disturbance d in Fig. 2). Each individual fault is designated as F_k^B with B being the aileron subsystem and k the specific fault magnitude (additive noise variance $\sigma^2 = k$ in Table 1). Such added noise leads to slightly noisy evolution of the “faulty” aircraft pitch rate after 6 sec [Fig. 3(b)].

Sequential Faults: Two types of LOE sequential faults affecting the elevator and aileron actuators are considered. The first one affects the elevator (referred to as F_{k_1, k_2}^C) and corresponds to sequential reductions of the position feedback gains P_1 and P_2 in the left elevator: The gain P_1 is reduced from 1 to k_1 at $t = t_1$, whereas P_2 reduces from 1 to k_2 at $t = t_2$ (with $t_2 > t_1$), as in Table 1. The aircraft’s pitch rate step response, when both reductions are present, is shown in Fig. 3(c).

The second sequential fault corresponds to decreases of the closed loop position feedback gain on both the left elevator and the left aileron circuits. The same reduction of P_2 as in the previous case in the left elevator (from 1 to k_1) is followed by a reduction (from 1 to k_2 , see Table 1) of the position feedback gain P_1 in the left aileron. This fault, referred to as F_{k_1, k_2}^D , also corresponds to equipment deterioration. The air-

craft's pitch rate step response, when both reductions are present, is shown in Fig. 3(d).

Remark: Both F_{k_1, k_2}^C and F_{k_1, k_2}^D may be seen as multiple faults caused by one specific malfunction (defective software, for instance), which is a similar idea to Common Mode Failures (CMF) ([13], ch.28 p.4). Such faults are rather unlikely to be accounted for during the initial design stage of the FDI algorithm. Hence, they may be referred to as *unmodelled*, as opposed to *modelled* faults which are accounted for during the FDI scheme's initial design. Thus, modelled faults may be both detected and identified, whereas unmodelled faults may, at best, be detected but not identified.

3 The Fault Detection and Identification Method

Aircrafts are highly nonlinear systems whose behavior varies with the flight regime (take off, clean flight or landing), the weight (and its distribution), environmental conditions (turbulence, weather) and other factors. The proposed FDI scheme (see Fig. 1) is centered around the nonlinear modelling of the relationships among measurable flight signals. A Multi-Input Single-Output (MISO) TFP-NARX representation (a Time-dependent Functionally Pooled NARX representation, that is with parameters being functions of time-dependent flight variables) describes the dependency among four signals: three taken as "inputs" (lateral and vertical accelerations and the angle-of-attack) and one as "output" (pitch rate). The TFP-NARX representation is identified from past flights, during an initial tuning phase referred to as the *baseline modelling phase* in the sequel (presented in section 3.1).

Once a TFP-NARX representation is identified, it is used *on-line* in any ongoing flight, during the *operational (or diagnostic) phase* (presented in section 3.2), to assess the current health state of the aircraft. If the actual system is in healthy state, the TFP-NARX model provides a one-step-ahead prediction of the output similar to the signal obtained from the simulator. The difference between the TFP-NARX model predic-

tion and the actual signal (the residual $e[t]$ in Fig. 1) will however change if a fault affects the aircraft (simulator). Then, the fault related information is extracted from $e[t]$ by means of a statistical decision-making strategy.

3.1 Baseline Modelling Phase

For a healthy aircraft, the dependency among the considered input-output signals is described by means of the following representation:

$$\begin{aligned} y_j[t] &= \sum_{i=0}^L \theta_i[t] \cdot p_{i,j}[t] + e_j[t] \quad \forall j \\ E\{e_j[t] \cdot e_i[t - \tau]\} &= \gamma_e[j, i] \delta[\tau] \quad \forall i, j \\ e_j[t] &\sim \text{NID}(0, \sigma_e^2(j)) \quad \forall j \end{aligned} \quad (1)$$

with t designating the normalized discrete time, $y_j[t]$ and $e_j[t]$ the model's output and one-step-ahead prediction error [or residual, assumed to be a zero-mean uncorrelated sequence with variance $\sigma_e^2(j)$] signals for the j -th flight, respectively. $E\{\cdot\}$ designates statistical expectation, $\text{NID}(\cdot, \cdot)$ Normally Independently Distributed (with the indicated mean and variance), $\delta[\tau]$ the Kronecker delta ($\delta[\tau] = 1$ when $\tau = 0$ and $\delta[\tau] = 0$ when $\tau \neq 0$) and $\gamma_e[j, i]$ the cross covariance ([14] pp. 409-411). The terms $p_{i,j}[t]$ are referred to as regressors and involve both the output $y_j[t]$ and the inputs(s) signals $u_{m,j}[t]$ (with m denoting the corresponding input). Each regressor term $p_{i,j}[t]$ may include polynomial functions of the output and/or the input signals, whereas by definition $p_{0,j}[t] \triangleq 1$. In each term, signal values of different lags may be admitted. The maximum lags of the signals $y_j[t]$, $u_{m,j}[t]$ in (1) (model orders) are n_y and n_{u_m} , respectively. The i -th regressor coefficient (model parameter) is noted $\theta_i[t]$ and is considered as function of relevant flight variables (hence it is time-varying).

The parameters $\theta_i[t]$ are considered as functions of relevant flight quantities $\ell_{1,j}[t]$, $\ell_{2,j}[t]$, \dots , $\ell_{q,j}[t]$ ($\ell_{i,j}[t]$ being the value of the quantity ℓ_i at time t for the j -th flight) as follows:

$$\begin{aligned} \theta_i(\ell_{1,j}[t], \ell_{2,j}[t], \dots, \ell_{q,j}[t]) &= \\ &= a_{i_0} + a_{i_1} \cdot \ell_{1,j}[t] + a_{i_2} \cdot \ell_{2,j}[t] + \dots + a_{i_q} \cdot \ell_{q,j}[t] \end{aligned} \quad (2)$$

The flight quantities $\ell_{1,j}[t]$, $\ell_{2,j}[t]$, \dots , $\ell_{q,j}[t]$, also referred to as basis functions, may be polynomial

functions of flight variables (such as the *Mach*, *Alt* and so on). The terms a_{i_0}, \dots, a_{i_q} denote the projection coefficients (assumed constant and common to all flights) of the i -th model parameter.

Discussion: The TFP-NARX representation (1) takes explicitly into account the multiple aircraft operating conditions (the M flights conducted under different conditions) during the system modelling phase: Data from *multiple* flights are treated as *one* entity (as shown in the sequel for the identification of a *single* representation). Thus, the pooled form of TFP-NARX representations is ideally suited to the (condition-dependent) aircraft dynamics. Naturally, if a single flight is considered, the TFP-NARX corresponds to a simple NARX model with time-dependent coefficients. The parameters $\theta_i[t]$ functionally depend upon important variables, as shown in (2). Hence, the resulting extra “flexibility” renders the TFP-NARX representation considerably “richer” than its conventional counterpart (that is, a Pooled NARX representation with Constant Coefficients or CCP-NARX, see [15]). Finally, the statistical dependencies among the different data records (flights) are easily accommodated into the model building (identification) phase: The second line of (1) points out that the residuals corresponding to two different flights j and i are potentially cross-correlated.

Identification: During the baseline phase the objective is: (a) To choose the regressors $p_{i,j}$ and the quantities $\ell_{i,j}$ that most accurately describe the system dynamics; (b) To estimate the associated parameters $\theta_i[t]$ or, equivalently, the coefficients of projection a_{i_0}, \dots, a_{i_q} . For this purpose, the top equation in (1) may be rewritten as¹:

$$y_j[t] = \underline{\phi}_j^T[t] \cdot \underline{\theta}[t] + e_j[t] \quad (3)$$

with $\underline{\phi}_j[t] = [p_{0,j}[t] \dots p_{L,j}[t]]^T$ and $\underline{\theta}[t] = [\theta_0 \dots \theta_L[t]]^T$ the parameter vector, respectively. The j -th flight data (N samples) may then be represented by a matrix equation similar in form to (3):

$$\underline{y}_j = \underline{\Phi}_j \cdot \underline{\theta}[t] + \underline{e}_j \quad (4)$$

with $\underline{y}_j \triangleq [y_j[1] \dots y_j[N]]^T \in \mathcal{R}^{[N \times 1]}$, $\underline{e}_j \triangleq [e_j[1] \dots e_j[N]]^T \in \mathcal{R}^{[N \times 1]}$ and $\underline{\Phi}_j = [\underline{\phi}_j[1] \dots \underline{\phi}_j[N]]^T \in \mathcal{R}^{N \times (L+1)}$. Let M be the number of flights (each of N recorded data samples) available for the tuning phase. For each of these flights, a matrix equation (4) may be defined. Pooling all M sets together (that is, stacking one on top each other) and using (4), yields the following matrix equation:

$$\underline{\bar{y}} = \underline{\bar{\Phi}} \cdot \underline{\theta}[t] + \underline{\bar{e}} \quad (5)$$

where $\underline{\bar{y}} \triangleq [\underline{y}_1^T \dots \underline{y}_M^T]^T \in \mathcal{R}^{[NM \times 1]}$ and $\underline{\bar{e}} \triangleq [\underline{e}_1^T \dots \underline{e}_M^T]^T \in \mathcal{R}^{[NM \times 1]}$. The matrix $\underline{\bar{\Phi}} \triangleq [\underline{\Phi}_1^T \dots \underline{\Phi}_M^T]^T \in \mathcal{R}^{[NM \times (L+1)]}$ involves the terms $p_{i,j}[t]$ for all M flights and all N time instants. Using (2) and (5), a matrix equation similar to (5) is obtained:

$$\underline{\bar{y}} = \underline{\Omega} \cdot \underline{\bar{\alpha}} + \underline{\bar{e}} \quad (6)$$

with $\underline{\bar{y}}$, $\underline{\bar{e}}$ as in (5) and $\underline{\bar{\alpha}} = [a_{1_0}, \dots, a_{1_q}, \dots, a_{L_0}, \dots, a_{L_q}] \in \mathcal{R}^{L(q+1) \times 1}$. If $\underline{1}_j[t] = [1, \ell_{1,j}[t], \dots, \ell_{q,j}[t]]^T$, the matrix $\underline{\Omega}$ is obtained as:

$$\underline{\Omega} = \begin{bmatrix} \underline{\phi}_1^T[1] \otimes \underline{1}_1^T[1] \\ \vdots \\ \underline{\phi}_1^T[N] \otimes \underline{1}_1^T[N] \\ \vdots \\ \underline{\phi}_M^T[1] \otimes \underline{1}_M^T[1] \\ \vdots \\ \underline{\phi}_M^T[N] \otimes \underline{1}_M^T[N] \end{bmatrix} \quad (7)$$

with \otimes designating the right *Kronecker* product.

The selection of $p_{i,j}$ and $\ell_{i,j}$ terms is performed in two stages. During the *first stage*, an *auxiliary* CCP-NARX representation of the system (see [15]) is considered, for the sole purpose of selecting the terms $p_{i,j}$ (using the data set of M flights) by means of a forward orthogonal search algorithm [16]. This auxiliary representation has a similar form to (5) but with a constant vector $\underline{\theta}$. The procedure is iterative and starts by searching the most significant regressor term. Once a term is selected, it is stored and the second most significant one is sought until a user-defined number

¹Underlined lower case/capital symbols designate column vector/matrix quantities, respectively.

of regressors is selected. Each term's significance is evaluated by its contribution to the reduction of the Residual Sum of Squares to Signal Sum of Squares (RSS/SSS) ratio. The term leading to the most significant RSS/SSS reduction is chosen at each iteration. During the *second stage*, the selected terms $p_{i,j}$ are utilized together with the previous data to select the $\ell_{i,j}$ functions (also using a forward search algorithm [17]) which best describe the system dynamics. The iterative procedure is the same as the one described above. Note, that selecting one set of quantities ($p_{i,j}$ or $\ell_{i,j}$) at a time means that, for a given system, an existing CCP-NARX structure may be converted to a (more effective) TFP-NARX one without resorting to a total system remodelling.

Finally, once both the $p_{i,j}$ and $\ell_{i,j}$ terms have been selected, the vector $\underline{\alpha}$ is estimated by using the form (6) and an Ordinary Least Squares (OLS) or a Weighted Least Squares (WLS) algorithm. For the given application, the selected $p_{i,j}$, $\ell_{i,j}$ and $\underline{\alpha}$ are presented in detail in section 4.1.

3.2 Operational (Diagnostic) Phase

The statistical tests used for FDI utilize the uncorrelatedness property of the healthy residual sequence $e[t]$. An l -sample long vector $[e[t - (l - 1)] \dots e[t]]$ (moving window) is considered at each time instant t , and the following hypothesis testing problem is constructed:

$$\begin{aligned} \mathcal{H}_0 : \rho_i = 0 \quad i = 1, \dots, r \quad (\text{healthy system}) \\ \mathcal{H}_1 : \rho_i \neq 0 \quad \text{for some } i \quad (\text{faulty system}) \end{aligned} \quad (8)$$

with \mathcal{H}_0 and \mathcal{H}_1 designating the null and alternative hypothesis. The term ρ_i designates the i -th correlation coefficient of the sequence $e[t]$ ([18] p. 55). Under the null hypothesis the following statistic follows χ^2 (chi-square) distribution with $(r - s + 1)$ degrees of freedom ([18], pp. 423-426):

$$Q = l \sum_{i=s}^r \hat{\rho}_i^2 \sim \chi^2(r - s + 1) \quad (9)$$

with $\hat{\rho}_i$ designating the estimated ρ_i and l the window length. The variable s is usually chosen equal to 1 ([18] p. 425). The hypothesis testing at the risk level α (that is the probability of rejecting

\mathcal{H}_0 given that \mathcal{H}_0 is true), is then formulated as:

$$\begin{aligned} Q < \chi_{(1-\alpha)}^2(r - s + 1) &\implies \mathcal{H}_0 \text{ is accepted} \\ \text{Else} &\implies \mathcal{H}_1 \text{ is accepted} \end{aligned} \quad (10)$$

with $\chi_{(1-\alpha)}^2$ the chi-square distribution's $(1 - \alpha)$ critical point. Clearly, the test (10) (referred to as *detection test A*) involves $(r - s + 1)$ coefficients of the statistical function (correlation) of $e[t]$.

An alternative test based upon the Partial Auto-Correlation Function (PACF), estimated for the residuals $e[t]$, is also constructed. The PACF Φ_{ii} , is the correlation between $e[t]$ and $e[t + i]$ after their mutual linear dependency on the intervening variables $e[t + 1]$, $e[t + 2]$, \dots , $e[t + i - 1]$ has been removed (see [14], pp. 67-68). To set up the test, the variable $\delta\hat{\Phi}_{ii} = \hat{\Phi}_{ii} - \Phi_{ii}^0$ is considered, with $\hat{\Phi}_{ii}$ being the partial correlation coefficient estimated at lag k for a data sequence (that is a l -long moving window of $e[t]$) and Φ_{ii}^0 an estimate of its mean value when the system is in healthy state. This estimate is obtained from a number of flights (other than those used for testing) conducted with an aircraft in healthy state. In general, due to disturbances, modelling errors and so on, a "small" (in magnitude) Φ_{ii}^0 (around 0.1) is an acceptable value. The following composite hypothesis testing problem for the true (but unknown) partial correlation coefficient is constructed:

$$\begin{aligned} \mathcal{H}_0 : \delta\Phi_{ii} = 0 \quad (\text{healthy system}) \\ \mathcal{H}_1 : \delta\Phi_{ii} \neq 0 \quad (\text{faulty system}) \end{aligned} \quad (11)$$

In practice, the PACF is estimated by fitting successive AutoRegressive (AR) models of orders $1, 2, \dots$ by OLS and retaining the last coefficient of each regression [14]. Then $\hat{\Phi}_{ii}$ is equal to the last coefficient of the estimated i -th order AR model. Furthermore, its variance is given by the (i, i) -th element of the parameter covariance matrix of the estimated AR model. It may be shown that the AR model parameter estimates follow normal distribution ([18] pp. 205-207). Hence, treating the estimated variance of $\hat{\Phi}_{ii}$ as a fixed quantity, the following function $Z = \frac{\delta\hat{\Phi}_{ii}}{\sqrt{\delta\sigma^2}}$ follows normal $\mathcal{N}(0, 1)$ distribution. Then, a test (referred to as *detection test B*) characterized by risk level α is

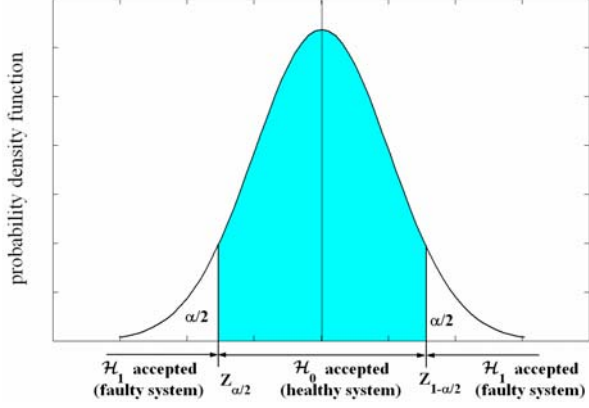


Fig. 4 : Statistical hypothesis test for $\delta\Phi_{ii}$ (the shaded area corresponds to accepting \mathcal{H}_0 at a risk level α).

formed:

$$\begin{aligned} Z_{\frac{\alpha}{2}} \leq Z \leq Z_{1-\frac{\alpha}{2}} &\implies \mathcal{H}_0 \text{ is accepted} \\ \text{Else} &\implies \mathcal{H}_1 \text{ is accepted} \end{aligned} \quad (12)$$

with $\delta\sigma^2$ designating the variance of $\delta\widehat{\Phi}_{ii}$ (which is equal to that of $\widehat{\Phi}_{ii}$) and Z_α the standard normal distribution's α critical point (see Fig. 4). Note, that both tests A and B can be used either for fault detection or fault identification.

4 Aircraft System FDI Results

4.1 Baseline Modelling Phase Results

Data are collected from $M = 99$ flights (other than those used for FDI testing) of 50 sec each, conducted inside the landing flight regime (data sampling rate 25 Hz) for a given aircraft configuration (no faults, constant weight-distribution and weather conditions). The auxiliary representation (see section 3.1) obtained is a CCP-NARX(10,[8 8 8]) model [that is, $n_y = 10$, $n_{u_m} = 8$ for $m = 1, 2, 3$], with $L = 70$. As stated in section 3.1, the choice of the regressors relies on the orthogonal algorithm in [16] and has been derived in [15] (where a simple CCP-NARX representation was used). The number of regressor terms and n_y , n_{u_m} are chosen on the basis of obtaining accurate prediction and approximate uncorrelatedness of the residual sequence $e[t]$, as well as satisfying some standard cross correlation tests between the input signals and the residuals [16].

Table 2 . The TFP-NARX(10,[8 8 8]) model structure (healthy system, landing flight regime, $W=31,850$ lbs, light turbulence).

$p_0 = 1$	$p_{35} = u_2[t-2]y[t-4]$
$p_1 = y[t-1]$	$p_{36} = u_1[t-6]y[t-9]$
$p_2 = y[t-2]$	$p_{37} = u_1[t-1]y[t-10]$
$p_3 = y[t-3]$	$p_{38} = u_2[t-3]u_2[t-3]$
$p_4 = y[t-4]$	$p_{39} = u_2[t-1]u_2[t-5]$
$p_5 = y[t-5]$	$p_{40} = u_2[t-2]u_2[t-4]$
$p_6 = y[t-6]$	$p_{41} = u_2[t-2]u_2[t-6]$
$p_7 = y[t-7]$	$p_{42} = u_2[t-5]u_2[t-8]$
$p_8 = y[t-9]$	$p_{43} = u_1[t-1]u_1[t-5]$
$p_9 = u_2[t-5]$	$p_{44} = u_1[t-1]u_1[t-7]$
$p_{10} = u_3[t-5]$	$p_{45} = u_1[t-1]u_1[t-6]$
$p_{11} = u_2[t-1]y[t-9]$	$p_{46} = u_1[t-1]u_1[t-3]$
$p_{12} = u_2[t-2]y[t-9]$	$p_{47} = u_2[t-6]u_3[t-1]$
$p_{13} = u_3[t-3]y[t-7]$	$p_{48} = u_2[t-5]u_3[t-2]$
$p_{14} = u_2[t-1]y[t-10]$	$p_{49} = u_2[t-1]u_2[t-4]$
$p_{15} = u_2[t-2]y[t-8]$	$p_{50} = u_2[t-6]u_3[t-2]$
$p_{16} = u_2[t-2]y[t-10]$	$p_{51} = u_2[t-2]u_3[t-3]$
$p_{17} = u_2[t-1]y[t-5]$	$p_{52} = u_2[t-1]u_3[t-5]$
$p_{18} = u_2[t-2]y[t-3]$	$p_{53} = u_2[t-1]u_3[t-2]$
$p_{19} = u_2[t-1]y[t-2]$	$p_{54} = u_2[t-3]u_3[t-3]$
$p_{20} = u_3[t-7]y[t-1]$	$p_{55} = u_2[t-3]u_3[t-8]$
$p_{21} = u_2[t-2]y[t-6]$	$p_{56} = u_2[t-4]u_2[t-8]$
$p_{22} = u_2[t-1]y[t-6]$	$p_{57} = u_1[t-4]u_3[t-8]$
$p_{23} = u_2[t-2]y[t-2]$	$p_{58} = u_1[t-4]u_2[t-7]$
$p_{24} = u_1[t-3]y[t-1]$	$p_{59} = u_2[t-1]u_3[t-8]$
$p_{25} = u_1[t-3]y[t-5]$	$p_{60} = u_2[t-2]u_3[t-2]$
$p_{26} = u_1[t-2]y[t-7]$	$p_{61} = u_2[t-3]u_3[t-5]$
$p_{27} = u_1[t-7]y[t-1]$	$p_{62} = u_2[t-5]u_3[t-3]$
$p_{28} = u_1[t-6]y[t-3]$	$p_{63} = u_2[t-3]u_3[t-1]$
$p_{29} = u_1[t-6]y[t-5]$	$p_{64} = u_2[t-5]u_3[t-1]$
$p_{30} = u_1[t-2]y[t-9]$	$p_{65} = u_2[t-1]u_2[t-6]$
$p_{31} = u_1[t-1]y[t-4]$	$p_{66} = u_1[t-4]u_2[t-3]$
$p_{32} = u_2[t-2]y[t-1]$	$p_{67} = u_2[t-4]u_3[t-1]$
$p_{33} = u_2[t-1]y[t-7]$	$p_{68} = y[t-5]y[t-10]$
$p_{34} = u_2[t-1]y[t-3]$	$p_{69} = y[t-1]y[t-1]$
$\ell_{1,j} = Mach^4$, $\ell_{2,j} = Alt \cdot Mach^3$, $\ell_{3,j} = Mach$,	
$\ell_{4,j} = Alt \cdot Mach^4$, $\ell_{5,j} = Mach^2$, $\ell_{6,j} = Alt \cdot Mach^3$	
$u_1[t]$: y-axis acceler. $u_2[t]$: z-axis acceler. $u_3[t]$: angle-of-attack AoA, $y[t]$: pitch rate q	

Table 3. Fault detection and identification results with tests A and B (low turbulence flights: 360; increased turbulence flights: 300).

Fault detection with test A (success rates %)					
Turb.	Healthy	F_k^A	F_k^B	F_{k_1,k_2}^C	F_{k_1,k_2}^D
low	89	93	100	100	100
increased	65	81	100	—	—
Fault detection with test B (success rates %)					
Turb.	Healthy	F_k^A	F_k^B	F_{k_1,k_2}^C	F_{k_1,k_2}^D
low	95	94	99	100	100
increased	89	83	96	—	—
Fault identification with test B (success rates %)					
Turb.	Healthy	F_k^A	F_k^B	F_{k_1,k_2}^C	F_{k_1,k_2}^D
low	n/a	100	100	—	
increased	n/a	100	100	n/a	n/a

n/a: not applicable

Using the auxiliary CCP-NARX(10,[8 8 8]) representation, a TFP-NARX model is derived, as described in section 3.1. The functional space is assumed to be spanned by polynomial functions of the aircraft altitude (Alt) and the $Mach$ number. The polynomial functions are subsequently inserted in a forward search algorithm [17] in order to select the most significant terms, shown at the bottom of Table 2. The selected model satisfies the majority of the standard validation tests, while obtaining accurate prediction [see Fig. 5(a), (b)].

4.2 Operational (Diagnostic) Phase Results

The testing procedure involves a total number of 360 flights (80 healthy, 80 with F_k^A , 140 with F_k^B , 30 with the F_{k_1,k_2}^C , 30 with F_{k_1,k_2}^D), all different from those employed in the TFP-NARX model building phase. Another 300 flights conducted under increased turbulence are studied in order to verify the scheme's robustness. The duration of each flight is equal to 100 seconds with a sampling rate of 25 Hz. The F_k^A and F_k^B faults enter the system right after $t = 20$ sec, whereas for the F_{k_1,k_2}^C and F_{k_1,k_2}^D the first fault is injected at $t_1 = 5$ sec and the second at $t_2 = 10$ sec (see section 2).

A 400 sample long moving window is used

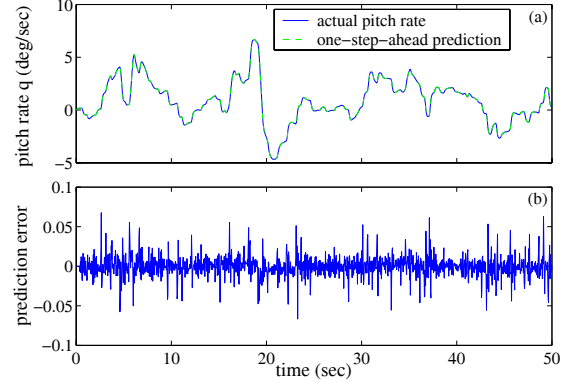


Fig. 5 : The identified TFP-NARX representation: (a) actual pitch rate versus one-step-ahead prediction, (b) one-step-ahead prediction errors (low turbulence, landing flight regime).

for FDI. Thus, the scheme is inoperative during the first 400 samples (≈ 16 sec). The detection and identification tasks are presented hereafter:

Fault Detection: The detection test A (10) is applied, with $\alpha = 10^{-5}$, $r = 35$ and $s = 2$ [see (9)]. The detection test B (12) is also employed on the same test flights, using the 2nd lag of the PACF (that is Φ_{22}). The results in Table 3 suggest that test A can be an adequate solution even for sequential (unmodelled) faults, but it is characterized by significant false alarm rates (11%). However, this comment is valid only for low turbulence conditions (see typical examples in Fig. 6). This is expected since the TFP-NARX representation is identified using low turbulence data.

In comparison, test B, also shown in Table 3, is notably better in terms of false alarms (5% versus 11% for test A) and missed detections. Most importantly, test B is more robust in increased turbulence conditions (F_k^A faults excepted). It should be noted that a small number (less than 20) of increased turbulence flights with sequential faults were conducted. The detection and false alarm performance remained almost unchanged, which is reasonable since these faults do not involve added noise (as in the F_k^B case). However, due to the small number of flights, the corresponding rates are not presented.

Hence, the most effective test (in a global sense) is test B. Note that the pooling procedure allows for including flights conducted under increased turbulence during the identification

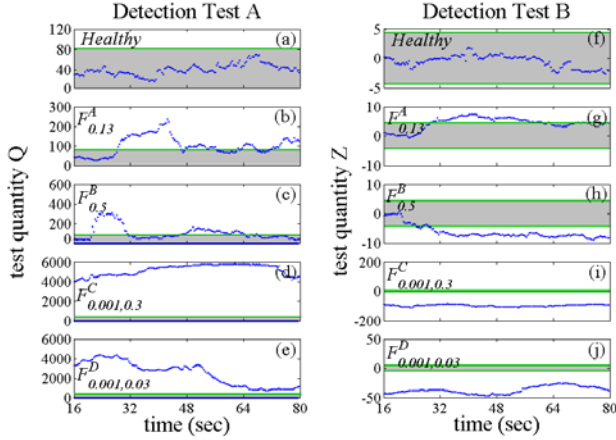


Fig. 6: Fault detection results: Test A (left column) and test B (right column) for typical flights under low turbulence (the shaded area corresponds to \mathcal{H}_0 ; $\alpha = 10^{-5}$).

phase, leading to improved FDI performance. Nevertheless, this was not done as the aim is to test the FDI scheme's robustness under harsh conditions.

Fault Identification: As noted in the previous paragraph, the statistical test offering the best global performance is the one based upon the PACF. It is thus chosen to perform fault identification, relying on the interesting observation that $\Phi_{22} > 0$ for flights affected by F_k^A faults, and $\Phi_{22} < 0$ for flights affected by F_k^B faults. Hence, the two fault types can be clearly distinguished. This leads to setting up a statistical test similar to (12). The main difference is that $\Phi_{22}^0 \equiv \Phi^*$ is an empirical mean value when the system is affected by the considered fault. As in the detection phase, the Φ^* value is computed from a number of flights not used in the testing phase. Then, for each of the F_k^A and F_k^B faults, two hypotheses are formulated: $\{\mathcal{H}_0$: system affected by a specific fault} and $\{\mathcal{H}_1$: system affected by another fault}. Furthermore, $\delta\Phi_{ii}^* = \Phi_{ii} - \Phi^*$ and the quantity $Z^* = \frac{\delta\hat{\Phi}_{ii}^*}{\sqrt{\delta\sigma^2}}$ [similar to Z in (12)] are readily defined, so that the following statistical test is performed:

$$\begin{aligned} Z_{\frac{\alpha}{2}} \leq Z^* \leq Z_{1-\frac{\alpha}{2}} &\implies \mathcal{H}_0 \text{ is accepted} \\ \text{Else} &\implies \mathcal{H}_1 \text{ is accepted} \end{aligned} \quad (13)$$

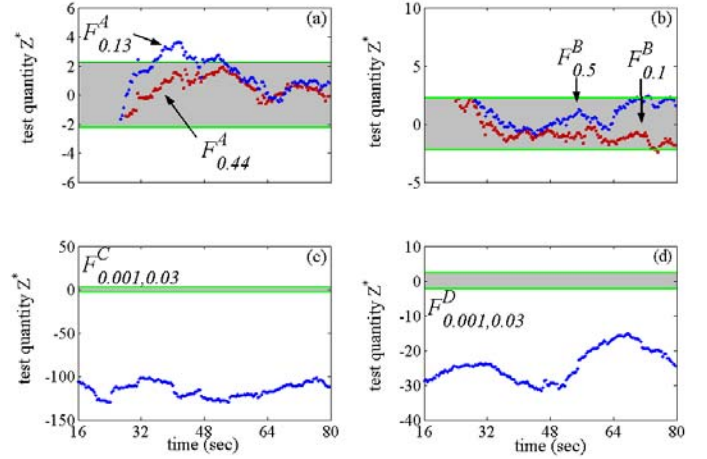


Fig. 7: Fault identification results with Test B for flights with low turbulence: (a) F_k^A faults; (b) F_k^B faults; (c) F_{k_1,k_2}^C fault; (d) F_{k_1,k_2}^D fault (the shaded area corresponds to identification of F_k^A , F_k^B , F_k^A and F_k^A faults, respectively; $\alpha = 0.025$).

The results in Table 3 show that the identification rates are also good for the modelled faults, even under increased turbulence conditions. Furthermore (as the typical examples in Fig. 7 show), no unmodelled faults are mistaken for modelled ones, and no F_k^A fault is identified as a F_k^B one. Note that the fault identification rates are based upon the number of flights detected as faulty during the detection phase. The robustness tests show that the FDI scheme gives decent results even for external conditions for which it has not been designed for (increased turbulence).

5 Conclusions

A scheme for the detection and identification of faults in aircraft systems has been presented. The scheme is based on a minimum of input-output data, and circumvents the need for hardware replication. This makes it suitable for systems requiring the optimal use of the on-board computing resources (like the future autonomous pilot-less aircraft). The MISO relation among specific flight signals (presently the vertical and horizontal acceleration, angle of attack and pitch rate) is modelled by means of TFP-NARX representations, with parameters being functions of

the *Alt* and *Mach* variables. FDI is then based upon the monitoring of the residuals produced from the identified model. The fault-related information is statistically evaluated via two tests (A and B).

Given the variety of magnitudes of the faults considered, the results are very promising: Faults were correctly detected and identified even under harsh external conditions (increased turbulence), which the scheme had not been designed for.

Acknowledgements

Research supported by the European Commission [STREP project No. 503019 on “Innovative Future Air Transport System (IFATS)”]. Thanks are due to the project partners, especially to Dr. M. Attar of IAI (Israel) for his useful comments.

References

- [1] Marcos A, Ganguli S and Balas G. An Application of \mathcal{H}_∞ Fault Detection and Isolation to a Transport Aircraft. *Control Engineering Practice*, Vol. 13, No. 1, pp 105-119, 2005.
- [2] Rago C, Prasanth R, Mehra R and Fortenbaugh R. Failure Detection and Identification and Fault Tolerant Control Using the IMM-KF with Applications to the Eagle-Eye UAV. *Proc. 35th IEEE Conf. Decision and Control*, Tampa, FL, 1998.
- [3] Zhang Y and Li X. Detection and Diagnosis of Sensor and Actuator Failures Using IMM Estimator. *IEEE Trans. Aerospace and Electronic Systems*, Vol. 34, No. 4, pp 1293-1313, 1998.
- [4] Zhang Y and Jiang J. Integrated Active Fault-Tolerant Control Using IMM Approach. *IEEE Trans. Aerospace and Electronic Systems*, Vol. 37, No. 4, pp 1221-1235, 2001.
- [5] Boskovic J and Mehra R. Multiple-Model Adaptive Flight Control Scheme for Accommodation of Actuator Failures. *J. Guidance, Control and Dynamics*, Vol. 25, No. 4, pp 712-724, 2002.
- [6] Samara P, Sakellariou J, Fouskitakis G and Fassois S. Detection of Sensor Abrupt Faults in Aircraft Control Systems. *Proc. IEEE Conference on Control Applications (CAA)*, Instabul, 2003 (extended version submitted for journal publication).
- [7] Attar M, Wahnou E and Chaimovitz D. Advanced Flight Control Technologies for UAVs. *Proc. 2nd AIAA Unmanned Unlimited Conference, Workshop and Exhibit*, San Diego, California, 2003.
- [8] Napolitano M, Neppach C, Casdorff V, Naylor S, Innocenti M and Silvestri G. Neural Network Based Scheme for Sensor Failure Detection, Identification and Accommodation. *J. Guidance, Control and Dynamics*, Vol 18, No. 6, pp 1280-1286, 1995.
- [9] Napolitano M, An Y and Seanor B. A Fault Tolerant Flight Control System for Sensor and Actuator Failures Using Neural Networks. *Aircraft Design*, Vol. 3, No. 1, pp 103-128, 2000.
- [10] Axelsson T. Diagnosis System Conceptual Design Utilizing Structural Methods Applied on a UAV's Fuel System, *LITH-ISY-EX-3552-2004*, Linkopings Univ., SE-581 83 Linkoping, 2004.
- [11] Zhang Q, Basseville M and Benveniste A. Fault Detection and Isolation in Nonlinear Dynamic Systems: A Combined Input-Output and Local Approach. *Automatica*, Vol. 34, No. 11, pp 1359-1374, 1998.
- [12] Samara P, Fouskitakis G, Sakellariou J and Fassois S. Aircraft Angle-of-Attack Virtual Sensor Design via a Functional Pooling NARX Methodology. *Proc. European Control Conference*, University of Cambridge, UK, 2003.
- [13] Spitzer C. *The Avionics Handbook*, CRC Press, 2001.
- [14] Box G, Jenkins G and Reinsel G. *Time Series Analysis Forecasting and Control*. 3rd Edition. Englewood Cliffs, NJ: Prentice Hall, 1994.
- [15] Dimogianopoulos D, Hios J, and Fassois S. Fault Detection and Isolation in Aircraft Systems Using Stochastic Nonlinear Modelling of Flight Data Dependencies. *Proc. Mediterranean Conference on Control and Automation MED 2006*, Ancona, Italy, 2006.
- [16] Billings S, Chen S and Korenberg M. Identification of MIMO Nonlinear Systems Using a Forward-Regression Orthogonal Estimator. *Int. J. of Control*, Vol. 49, No. 6, pp 2157-2189, 1989.
- [17] Haber R and Unbehauen H. Structure Identification of Nonlinear Dynamic Systems - A Survey on Input/Output Approaches. *Automatica*, Vol. 26, No. 4, pp 651-677, 1990.
- [18] Söderström T and Stoica P. *System Identification*. London: Prentice Hall-Int., 1989.